JOURNAL OF GEOPHYSICAL RESEARCH, VOL. 106, NO. A9, PAGES 18,789–18,802, SEPTEMBER 1, 2001

A global MHD and empirical magnetic field model investigation of the magnetospheric cusp

F. R. Fenrich,[1,2] J. G. Luhmann,[1] J. A. Fedder,[3] S. P. Slinker,[4] and C. T. Russell[5]

Abstract. Magnetic field configurations, cusp locations, merging, and interconnection regions for the Lyon-Fedder global magnetohydrodynamic (MHD) simulation model and the Tsyganenko 96 (T96_01) empirical model are presented and compared for three different interplanetary magnetic field (IMF) directions (north, south, and dusk directed). Field line configurations indicate a significantly larger magnetosphere in the T96_01 model compared to the MHD model for all IMF directions. In each of the models the polar cusp is identified by depressions in the magnetic field residual and by the boundary between dayside closed and open field lines. It is found that the MHD model exhibits a much stronger residual magnetic field depression in the cusp region than does the T96_01 model. The MHD field depression is associated with the presence of diamagnetic magnetosheath plasma that enters the cusp via the MHD merging process. In the northward IMF case, MHD merging above both poles results in an MHD open-closed field line boundary located at 89° invariant latitude with MHD cusp plasma and field depressions centered on closed field lines near 81°. The T96_01 model is very different from this with its north IMF open-closed boundary located at 79° invariant latitude. For the southward IMF case the T96_01 open-closed boundary at 74° invariant latitude lies slightly poleward of the MHD open-closed boundary at 73°. In this case the MHD cusp plasma is centered near 75° invariant latitude. In the dusk-directed IMF case the MHD cusp plasma shifts ~2 hours in magnetic local time (MLT) toward dusk and remains poleward of the MHD open-closed boundary. In this case the MHD dayside open-closed boundary extends from dawn to dusk, while the T96_01 dayside open-closed boundary extends only from dawn to ~13 MLT and near local noon is coincident with the MHD boundary at ~74° invariant latitude. Differences between the two models are due in large part to differences in the form of their interconnectivity with the interplanetary magnetic field lines. For each IMF direction the MHD merging locations and T96_01 strongest interconnection regions are identified and are found to be very different. On the basis of comparisons with numerous case and statistical studies of the cusp it is concluded that the MHD model provides a fairly realistic representation of the cusp and dayside magnetic field configuration, while the T96_01 model is limited in its ability to model the cusp region.

1. Introduction

Global magnetospheric models are important tools in the study of the interaction between the solar wind and the magnetosphere. They provide visualization of the solar wind control of magnetospheric configuration and are needed for field line mapping and particle trajectory studies. Used in conjunction with observational data they can provide additional insight into the physical processes at work in the magnetosphere. Given the common use of empirical models and the increasing popularity of MHD models it is important to evaluate the similarities and differences in these two model types.

There are several global MHD numerical simulation models currently in use today [e.g., *Fedder and Lyon,* 1995; *Gombosi et al.*, 1998; *Raeder et al.*, 1995; *White et al.,* 1998; *Ogino*, 1986; *Tanaka*, 1995], each with its own particular numerical simulation method, grid spacing, resistivity, and boundary conditions. Such MHD models have been used to investigate magnetospheric configuration and solar wind coupling processes for a variety of solar wind conditions, including northward interplanetary magnetic field (IMF) [*Gombosi et al.*, 1998; *Raeder et al.*, 1995; *Ogino*, 1986, *Fedder and Lyon*, 1995], southward IMF [*Fedder et al.*, 1995; *Ogino*, 1986], and *y*-directed IMF [*White et al.,* 1998; *Crooker et al.,* 1998; *Fedder et al.,* 1997; *Ogino et al.,* 1986; *Tanaka,* 1999]. Some of the most commonly used empirical models are the Tsyganenko models [*Tsyganenko*, 1987, 1989, 1996], which are all data based. The most recent of these is the T96 model, which is controlled by solar wind inputs.

[1]Space Sciences Laboratory, University of California, Berkeley, California.
[2]Now at Department of Physics, University of Alberta, Edmonton, Alberta, Canada.
[3]Institute for Computational Sciences and Informatics, George Mason University, Fairfax, Virginia.
[4]Plasma Physics Division, Naval Research Laboratory, Washington, D. C.
[5]Institute of Geophysics and Planetary Physics, University of California, Los Angeles, California.

Paper number 2001JA900040.
0148-0227/01/2001JA900040$09.00

In this paper we concentrate primarily on the polar cusp region, which is the critical region through which a large proportion of the solar wind mass and energy enter the magnetosphere. Current definitions of the cusp are somewhat variable being dependent upon the location and method of observation. At low altitudes it is generally accepted that the cusp can be separated into two morphologically distinct regions known as the cusp proper and the cleft [*Newell and Meng*, 1988; *Kremser and Lundin*, 1990]. The cusp proper is that region comprising the most direct entry of magnetosheath plasma and is identified by high number flux and low average ion and electron energies, while the cleft is characterized by lower densities but higher average ion and electron energies and is believed to map to the low-latitude boundary layer (LLBL). At high altitudes the cusp is currently being monitored by the Polar spacecraft. Using data from the Polar Magnetic Fields Experiment (MFE), Hot Plasma Analyzer (HYDRA) and Toroidal Imaging Mass-Angle Spectrograph (TIMAS) instruments, *Zhou et al.* [1997, 1999, 2000] are identifying the cusp by depressions in the total magnetic field residuals and enhancements in magnetosheath-like plasma densities. Given the different identification criteria by different instruments at different altitudes and the cusps large variability with solar wind and IMF conditions, many aspects of the location and the dynamics of the cusp remain in question. Global magnetospheric models can provide a controlled means of studying the cusp and its dependence on solar wind and interplanetary magnetic field.

The goal of this work is to compare two different magnetospheric models in terms of their magnetic field configurations and cusp locations for three different interplanetary magnetic field orientations including northward ($+B_z$), southward ($-B_z$), and duskward ($+B_y$) IMF directions. The first model is the Tsyganenko 96 (T96_01) model, which is a data-based empirical model controlled by input solar wind parameters [*Tsyganenko*, 1996; *Tsyganenko and Stern*, 1996; *Tsyganenko*, 1995]. The second model is the magnetohydrodynamic (MHD) numerical simulation model developed by *Fedder and Lyon* [1987, 1995]. After a description of the Lyon-Fedder MHD model and the T96_01 model and each of their limitations, their magnetospheric configurations will be compared using field line tracings, total magnetic field residuals, and external field measurements along a simulated Polar spacecraft trajectory. Since the T96_01 model exhibits limited residual field depressions in the cusp region, the cusp locations will be quantified and compared using dayside open-closed field line boundaries. According to *Dungey*'s [1961, 1963] model the cusp is poleward of the open-closed boundary for southward IMF and equatorward of the boundary for northward IMF. Weak field magnetopause regions resulting from MHD merging and T96_01 interconnectivity are also compared. The results will be discussed in terms of previous case and statistical studies of the cusp.

2. Model Descriptions

The Fedder-Lyon MHD global simulation model is a three-dimensional numerical solution of the ideal MHD equations. The simulations are a self-consistent, time-dependent model of the solar wind-magnetosphere-ionosphere system. The numerical mesh is an irregular computer-generated grid with outer boundaries at x=30 R_E and -300 R_E, and $(y^2 + z^2)^{1/2}$=60 R_E. The inner boundary is at a radial value of 3.5 R_E. For further details of this model see *Fedder and Lyon* [1987, 1995] and *Fedder et al.* [1995]. For this study the raw simulation results have been interpolated to a regular grid with a resolution of 0.5 R_E in each direction and outer limits at x=-10 R_E, x=15 R_E, and $|y|=|z|$=20 R_E. The following steady solar wind conditions were used in the simulations presented: plasma number density, n=6.5 cm^{-3}; solar wind velocity, v=400 km s^{-1}; and magnetic field strength, $|B|$=5 nT for the north and south IMF cases and $|B|$=10 nT for the dusk IMF case.

The T96_01 model is a data-based global model of the magnetospheric magnetic field with an explicitly defined magnetopause controlled by the solar wind pressure. It incorporates large-scale regions 1 and 2 Birkeland current systems and IMF penetration across the boundary. The model requires the following input parameters: solar wind dynamic pressure (P_{dyn}), *Dst* index, y and z components of the interplanetary magnetic field, and the geodipole tilt angle. For this study the required parameters were chosen to be consistent with the parameter values in the MHD simulation model. For the north IMF case, P_{dyn}=1.7 nPa, *Dst*=0, B_y=0, and B_z=+5 nT. For the south IMF case, P_{dyn}=1.7 nPa, *Dst*=-50 nT, B_y=0, and B_z=-5 nT. For the duskward IMF case, P_{dyn}=1.7 nPa, *Dst*=0 nT, B_y=+10 nT, and B_z=0. In all cases the dipole tilt angle was taken to be zero. The total T96_01 model includes the T96_01 external field plus an internal dipole field corresponding to the epoch of 1980.

Note that in the T96_01 model the *Dst* was chosen to be zero for the northward and duskward IMF cases to model the fact that little ring current is generated during such IMF conditions. However, with *Dst*=0 nT there will remain a residual T96_01 ring current related to dynamic pressure. For the southward IMF case a *Dst*=-50 nT was chosen to model the existence of a significant ring current during periods of IMF B_z=-5 nT.

Although MHD models have the advantage of self-consistency and the explicit inclusion of plasma effects, they can be limited by the boundary conditions, plasma sources, and resistivity values chosen. Such limitations are not always essential for MHD but rather are dependent upon the form of the particular MHD model. In the Lyon-Fedder MHD model used here, no explicit resistivity is included, the ionospheric conductivities are fixed, and all of the plasma in the model originates from the solar wind with no ionospheric sources. No realistic ring current develops in the model in part because of the lack of an ionospheric source of plasma but more importantly because of the MHD assumption that the bulk of the plasma can be described as a density and a temperature. The real ring current is composed in the high-energy tail of the ion distribution function. This MHD model does not yet include the plasma energy distribution required for realistic ring current development. The simulation grid spacing in the Lyon-Fedder MHD model does increase toward the downtail boundary increasing the numerical viscosity there. However, this has a negligible effect upon magnetotail dynamics and the simulation results overall. The reconnection that occurs in the Lyon-Fedder model is numerical in origin, resulting from the averaging of oppositely directed fields. However, the reconnection rate and location are controlled by the physical boundary conditions and not by the local value of numerical resistivity [*Fedder and Lyon*, 1987].

The T96_01 model has the following set of limitations. It

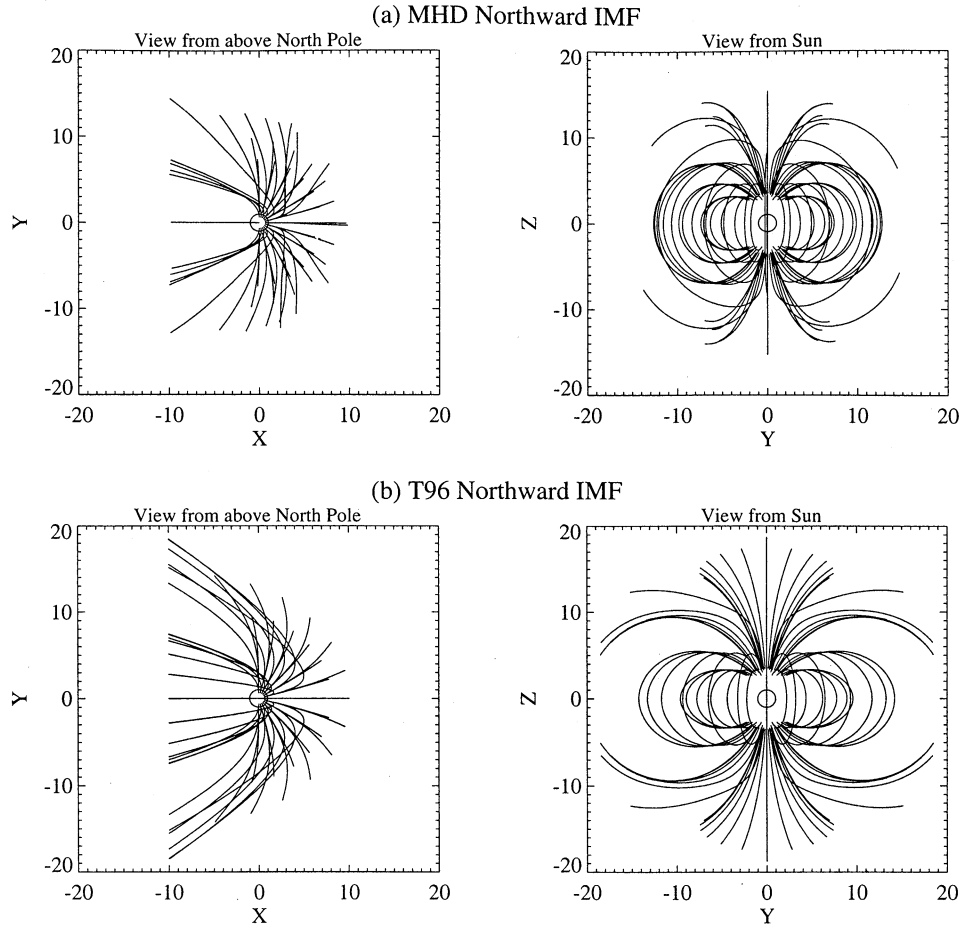

Figure 1. Dayside magnetic field line tracings for (a) the MHD model and (b) the T96_01 model for the northward IMF case. The field lines have been traced outward from the inner boundary at 3.5 R_E in 10° increments from 50° latitude to 90° latitude and in increments of 15° longitude from dawn to dusk. Figures 1a and 1b (left) show the field line tracings as viewed from above the North Pole, and Figures 1a and 1b (right) show the field line tracings as viewed from the Sun. Note that the field line tracings end at x=-10 R_E and $|y|=|z|=20$ R_E as these are the limits for the MHD grid.

is a data based model and is thus limited by the available data coverage. Regions lacking sufficient constraining data will not be correctly modeled. The T96_01 model has a specified configuration of current systems, which has little flexibility and may not include all possible current systems. For example, in the T96_01 model the location of the region 1 and region 2 field-aligned currents at low altitude are specified in accordance with the results of *Iijima and Potemra* [1976], which are a statistical average and thus do not allow any variability with IMF direction. In the T96_01 model, there is no opportunity for a self-consistent adjustment of the fields and currents. The size and shape of the T96_01 magnetopause boundary are explicitly defined and are controlled only by the solar wind dynamic pressure. The resulting magnetopause is similar to that deduced from direct observations of the magnetopause crossings by *Sibeck et al.* [1991] but does not take into account variations in magnetopause location resulting from changes in the IMF direction. Finally, the T96_01 model assumes that the interconnection field preserves the solar wind magnetic field direction but varies in magnitude with distance from the subsolar point along the x axis and with the distance from the plane containing the Sun-Earth line and the IMF vector. External to the magnetosphere the fields are purely the interconnection fields and thus are not necessarily representative of magnetosheath or solar wind fields.

3. Model Results and Comparisons

Figures 1, 2, and 3 illustrate the MHD magnetic field configurations and the T96 dayside magnetic field configurations for the north, south, and dusk-directed IMF, respectively. One of the more notable differences between the two model configurations is the fact that the T96_01 magnetosphere is larger than the MHD magnetosphere in terms of the subsolar distance, height, and width. Unlike the global MHD simulation, the T96_01 model does not include a magnetosheath. Thus the magnetic field outside of the T96_01 magnetopause is not to be taken as representing anything but the interconnection field specified in the empirical T96_01 model. Nevertheless, the field near the magnetopause can be compared with the MHD results to investigate whether the form of the interconnection field in T96_01 looks anything like the self-consistent MHD

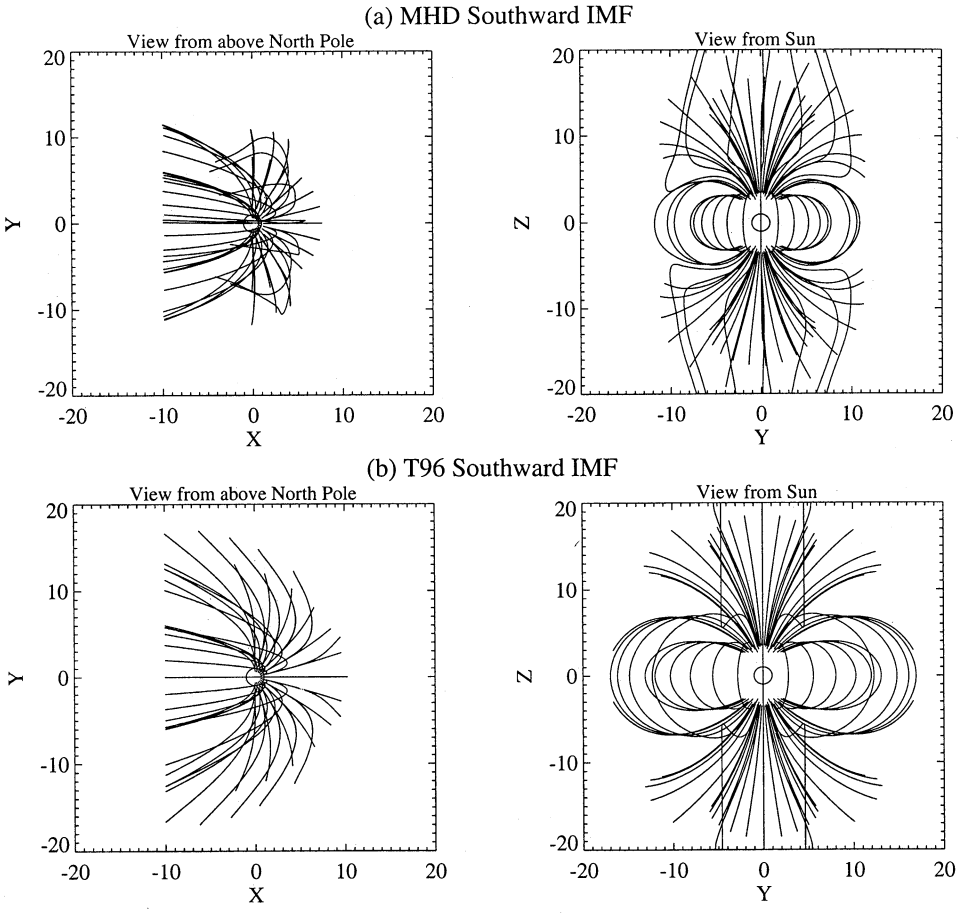

Figure 2. Dayside magnetic field line tracings for (a) the MHD model and (b) the T96_01 model for the southward IMF case. The field lines have been traced outward from the inner boundary at 3.5 R_E in 10° increments from 50° latitude to 90° latitude and in increments of 15° longitude from dawn to dusk. Figures 2a and 2b (left) show the field line tracings as viewed from above the North Pole, and Figures 2a and 2b (right) show the field line tracings as viewed from the Sun.

simulation. It is apparent from Figures 1-3 that the MHD open fields near the magnetopause are very different from the T96_01 interconnection fields.

Figures 4a and 4b show field lines traced from foot points in the noon-midnight plane for the northward IMF MHD and T96_01 models, respectively. The solid lines are traced from the inner boundary at 3.5 R_E in 5° increments beginning at 15° latitude. Also included as a solid line is the last closed field line traced outward from the Northern Hemisphere. The dashed lines represent purely solar wind/magnetosheath field lines in the MHD model and interconnection fields in the T96_01 model. In Figures 4a and 4b the gray scale represents the total magnetic field residual obtained by subtracting the internal dipole field strength from the total model field strength. Thus the darker gray areas represent areas of magnetic field depression. Note that there are gray regions outside the magnetopause because the internal dipole field strength in these regions is greater than the magnetosheath or solar wind field strength in the case of MHD or greater than the interconnection field in the case of T96_01. The long-dashed lines in Figures 4a and 4b indicate a simulated Polar spacecraft trajectory over the North Pole along the noon-midnight meridian. The residual fields along this trajectory are plotted in Figure 4c with the solid line representing the MHD residual fields and the dashed line representing the T96_01 residual fields. Similar plots for the southward and duskward IMF cases are shown in Figures 5 and 6.

It is apparent in Figures 4, 5, and 6 that there is a much larger and deeper penetrating cusp magnetic field depression in the MHD model, Figures 4a, 5a, and 6a, compared to the T96_01 model, Figures 4b, 5b, and 6b. The bottom plot of Figures 4c, 5c, and 6c also illustrates the model differences in the total magnetic field residuals along the simulated Polar spacecraft trajectory. Note that in the MHD model the maximum field depression ranges from –50 nT to –60 nT, while in the T96_01 model the maximum field depression is approximately -25 nT at high altitudes with little or no field depression at Polar spacecraft altitudes. The regions of MHD cusp field depression are collocated with regions of enhanced plasma density due to pressure balance and the diamagnetic effects of the MHD cusp plasma. Since the T96_01 model includes no explicit plasma, the effects of cusp plasma in this model are only realized through the model's fit to observations. In the T96_01 model, there is no strong cusp field depression, which may be an indication that there is an insufficient database in the cusp region and possibly that the

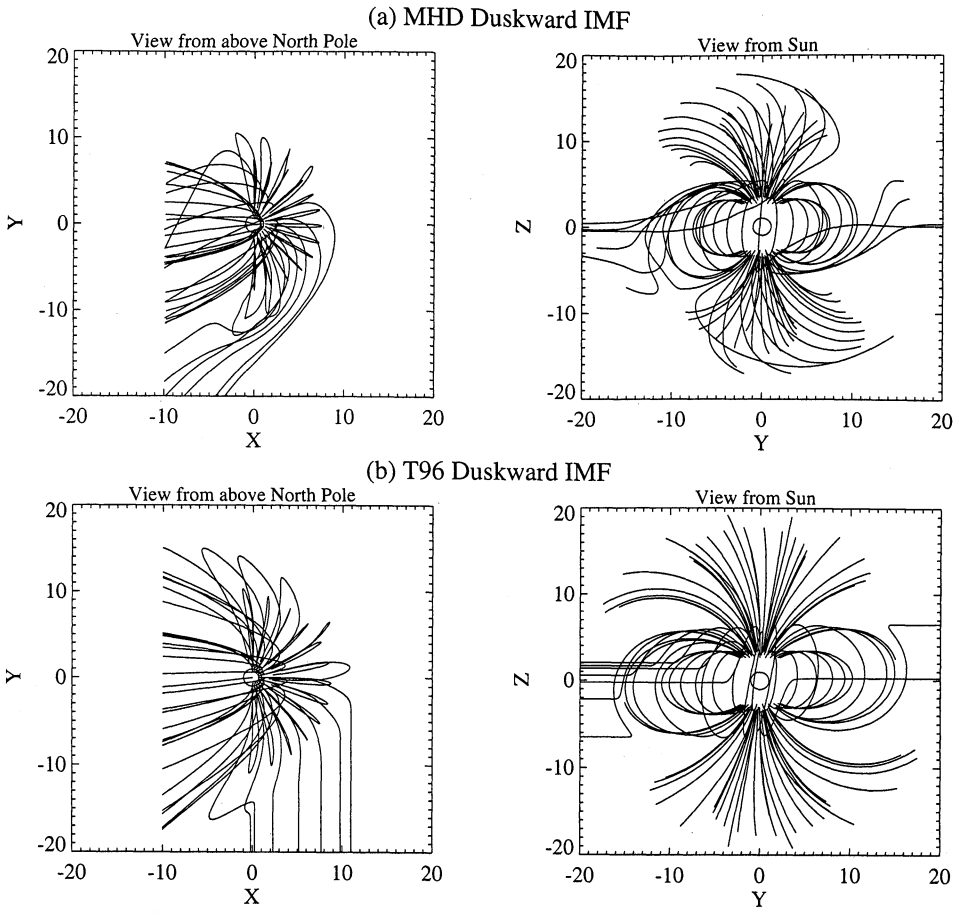

Figure 3. Dayside magnetic field line tracings for (a) the MHD model and (b) the T96_01 model for the duskward IMF case. The field lines have been traced outward from the inner boundary at 3.5 R_E in 10° increments from 50° latitude to 90° latitude and in increments of 15° longitude from dawn to dusk. Figures 3a and 3b (left) show the field line tracings as viewed from above the North Pole and Figures 3a and 3b (right) show the field line tracings as viewed from the Sun.

specified forms of the current systems are unable to model diamagnetic cusp currents. In all cases for both models except the MHD northward IMF case the maximum in the field depression occurs near the bifurcating field line that separates the forward dayside bending field lines from the backward nightside bending field lines. In the MHD north IMF case the bifurcating field line is poleward of the peak in the field depression.

In Figure 6c a large B_y residual is seen throughout the cusp region in the MHD duskward IMF model that is not present in the T96_01 model. This large B_y residual is due to a strong field-aligned current system generated by the interaction of the duskward IMF with the magnetosphere. The nonexistence of such y directed fields in the T96 model is an indication that the T96_01 model does not include such a field-aligned current system. The large total magnetic field depressions and the large negative B_z residuals in the equatorial region of the T96_01 model (see Figures 4b, 4c, 5b, 5c, 6b, and 6c) are due to the presence of a ring current which is absent in the MHD model.

It is apparent in Figures 4, 5, and 6 that the form of the solar wind/magnetosheath field just outside the magnetopause is very different in each of the two models. Recall that the T96_01 model has only its interconnection field outside of the magnetosphere, whereas the MHD model has a magnetosheath region where the IMF field lines bend to conform to the shape of the magnetosphere. These plots illustrate the different forms of interconnectivity between the geomagnetic field and the IMF for the two models. Note that in the MHD northward IMF case, Figure 4a, the field line tracings indicate that magnetic merging between solar wind field lines and geomagnetic lobe field lines is occurring above both poles, resulting in closed field lines of solar wind origin.

A quantitative comparison of the model cusp locations can be achieved using the boundaries between dayside closed and open field lines. Figure 7 shows polar plots of the magnetic local time (MLT) versus invariant latitude locations of the dayside open-closed field line boundaries for the northward IMF case (Figure 7a), the southward IMF case (Figure 7b), and the duskward IMF case (Figure 7c) for each model. Note than in all T96_01 model cases and the MHD north case the boundaries do not span the entire dawn to dusk range. This is because the open-closed boundaries shown correspond only to those field lines that become open to the solar wind sunward of -10 R_E and do not include the transition from closed to open lobe field lines. Figure 7 also includes the 6 and 10 cm^{-3} plasma density contours determined at 6 R_E in the MHD model and traced down to ionospheric heights.

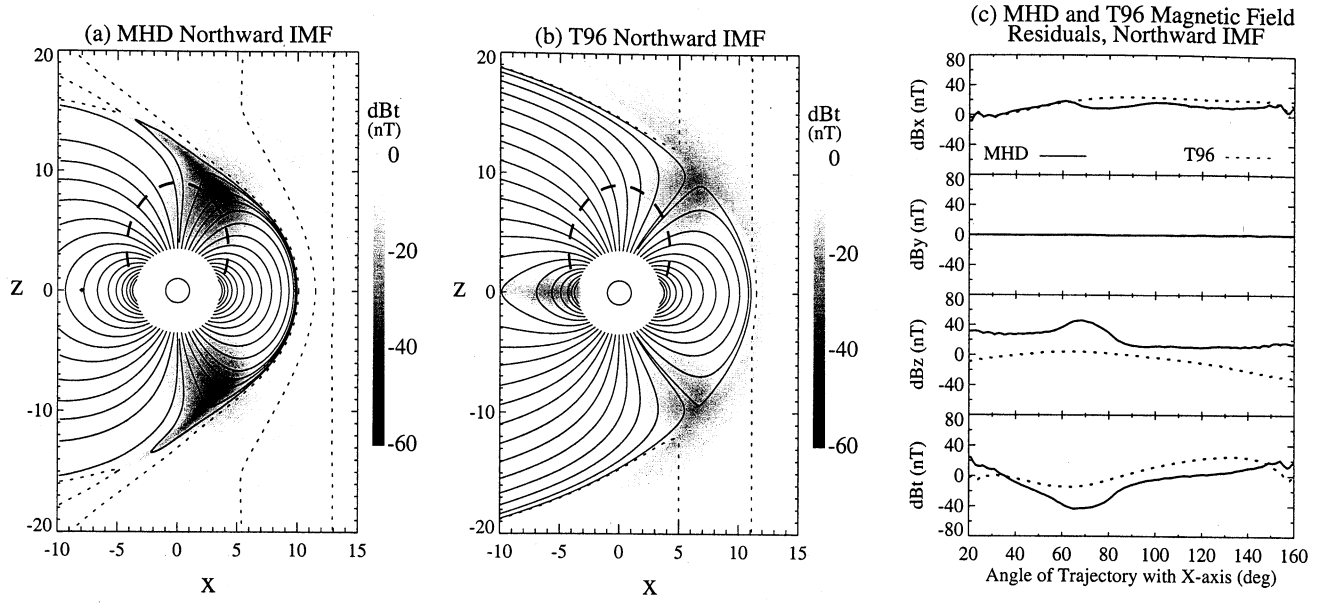

Figure 4. Northward IMF case: total magnetic field residuals and field line tracings from the noon-midnight meridian for (a) the MHD model and (b) the T96 model. The solid lines are traced from the inner boundary at 3.5 R_E in 5° increments beginning at 15° latitude. Also included as a solid line is the last closed field line traced outward from the Northern Hemisphere. The short-dashed lines represent solar wind/magnetosheath field lines in the MHD model and interconnection fields in the T96_01 model. The gray scale represents the total magnetic field residuals obtained by subtracting the internal dipole field strength from the total magnetic field strength. The long-dashed lines indicate a simulated Polar spacecraft trajectory over the North Pole in the noon-midnight meridian. The residual fields along this trajectory are shown in Figure 4c with solid lines representing the MHD model and dashed lines representing the T96_01 model.

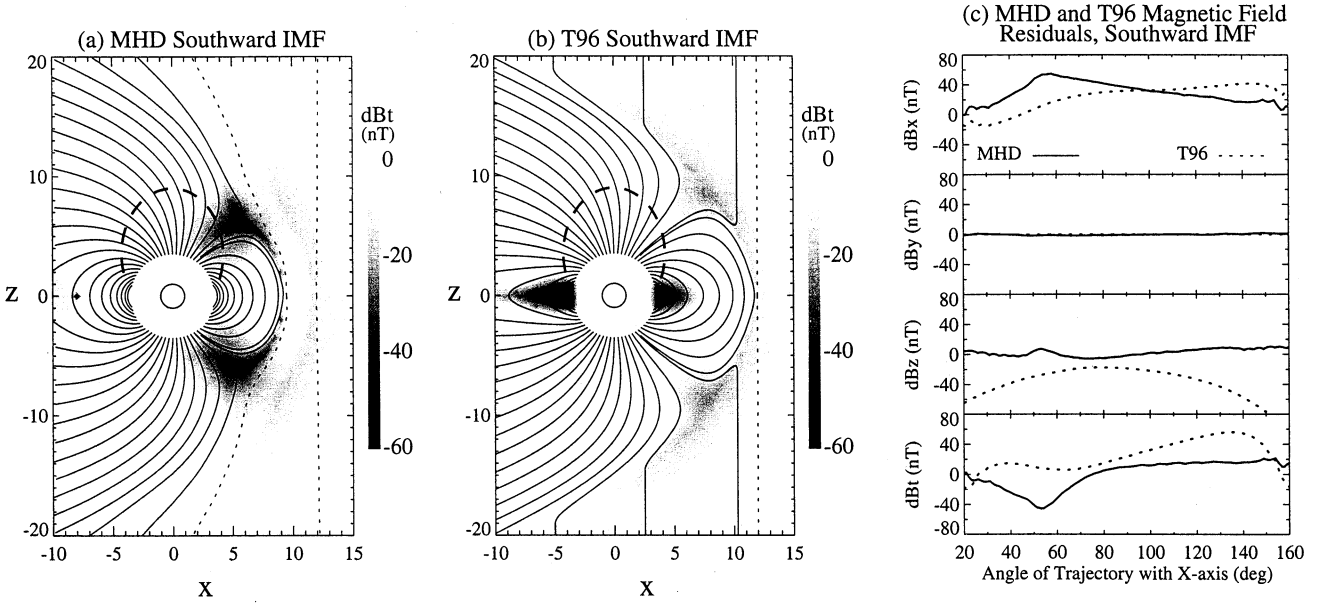

Figure 5. Southward IMF case: total magnetic field residuals and field line tracings from the noon-midnight meridian for (a) the MHD model and (b) the T96 model. The solid lines are traced from the inner boundary at 3.5 R_E in 5° increments beginning at 15° latitude. Also included as a solid line is the last closed field line traced outward from the Northern Hemisphere. The short-dashed lines represent solar wind/magnetosheath field lines in the MHD model and interconnection fields in the T96_01 model. The gray scale represents the total magnetic field residuals obtained by subtracting the internal dipole field strength from the total magnetic field strength. The long-dashed lines indicate a simulated Polar spacecraft trajectory over the North Pole in the noon-midnight meridian. The residual fields along this trajectory are shown in Figure 5c with solid lines representing the MHD model and dashed lines representing the T96_01 model.

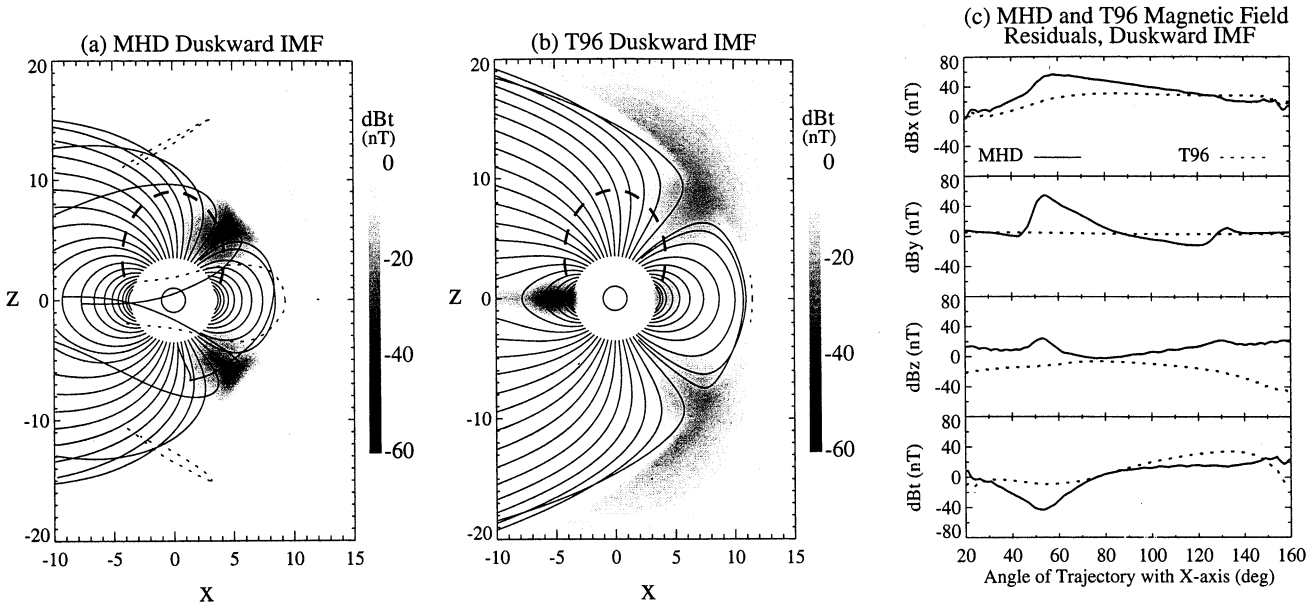

Figure 6. Duskward IMF case: total magnetic field residuals and field line tracings from the noon-midnight meridian for (a) the MHD model and (b) the T96 model. The solid lines are traced from the inner boundary at 3.5 R_E in 5° increments beginning at 15° latitude. Also included as a solid line is the last closed field line traced outward from the Northern Hemisphere. The short-dashed lines represent solar wind/magnetosheath field lines in the MHD model and interconnection fields in the T96_01 model. The gray scale represents the total magnetic field residuals obtained by subtracting the internal dipole field strength from the total magnetic field strength. The long-dashed lines indicate a simulated Polar spacecraft trajectory over the North Pole in the noon-midnight meridian. The residual fields along this trajectory are shown in Figure 6c with solid lines representing the MHD model and dashed lines representing the T96_01 model. Note that many of the field lines in Figures 6a and 6b exit the noon-midnight plane.

In the northward IMF case shown in Figures 4a, 4b, and 7a, the MHD dayside open-closed field line boundary is located at ~89° invariant latitude poleward of the MHD cusp plasma and field depression and far poleward of the T96_01 open-closed boundary at ~79° invariant latitude. The reason for this large difference between the models is that in the MHD simulation reconnection occurs above the poles, allowing diamagnetic magnetosheath plasma to enter and flow down the newly closed field lines in the sunward direction. This places the MHD cusp plasma deep on closed field lines in the northward IMF case. The location of the MHD cusp plasma which results in diamagnetic field reduction is very close to the *Newell et al.* [1989] statistical cusp to be discussed in section 4. On the other hand, the T96_01 model has an interconnection field at the magnetopause which decreases with distance from the subsolar point. Thus its region of strongest interconnectivity is sunward of the Earth, resulting in an open-closed boundary located at much lower latitudes than is the open-closed boundary of the MHD model.

For the southward IMF case shown in Figures 5a, 5b, and 7b the MHD open-closed boundary shifts equatorward to ~73° invariant latitude at local noon, while the T96_01 boundary shifts to ~74° invariant latitude. Here the MHD cusp plasma and field depression and the T96_01 bifurcation region are just poleward of their respective open-closed boundaries.

In the dusk-directed IMF case, Figures 6a, 6b, and 7c, the MHD open-closed boundary has a noon location of ~74° invariant being slightly equatorward in the dawn sector and slightly poleward in the dusk sector. The MHD cusp plasma shifts duskward and is on open field lines. The T96_01 boundary is coincident with the MHD model boundary at local noon but spans just the dawn sector a degree or two equatorward of the MHD boundary. Thus, in the dusk directed IMF case the models exhibit different types of dawn-dusk asymmetry. In the T96_01 model the open-closed boundary shifts dawnward, while in the MHD model the cusp plasma shifts significantly duskward with no strong asymmetry seen in the open-closed boundary.

To illustrate where the open-closed boundaries map to in the outer magnetosphere, sample tracings of the last closed and first open field lines along this boundary are shown in Figures 8, 9, and 10 for the north, south, and dusk-directed IMF, respectively. Note that in the northward and southward IMF cases the MHD model boundary tracings extend much further along the dawnward and duskward flanks than does the T96_01 model. In the duskward IMF case both models show open field lines that connect to the dawn side; however, in the MHD model the foot points of these field lines extend to near dusk local times, whereas in the T96_01 model they do not extend much past noon magnetic local time.

The model results outlined above illustrate that the cusp locations and overall magnetospheric configurations are controlled by the solar wind IMF direction. One of the primary mechanisms by which the solar wind exerts its control of the magnetosphere is via the process of magnetic merging on the dayside magnetopause. In the MHD model, merging is numerical and occurs because of numerical

(a)Dayside Open-Closed Boundaries and MHD Cusp Plasma Northward IMF

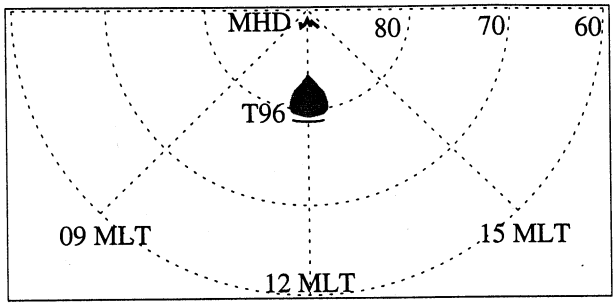

(b) Dayside Open-Closed Boundaries and MHD Cusp Plasma Southward IMF

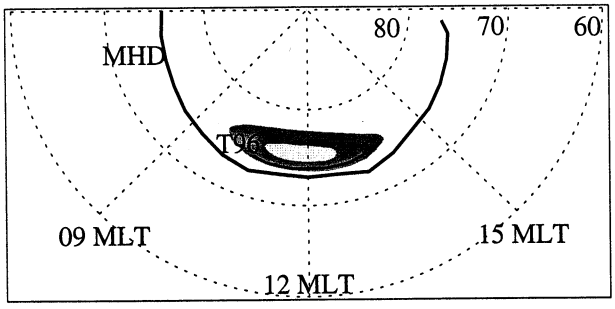

(c) Dayside Open-Closed Boundaries and MHD Cusp Plasma Duskward IMF

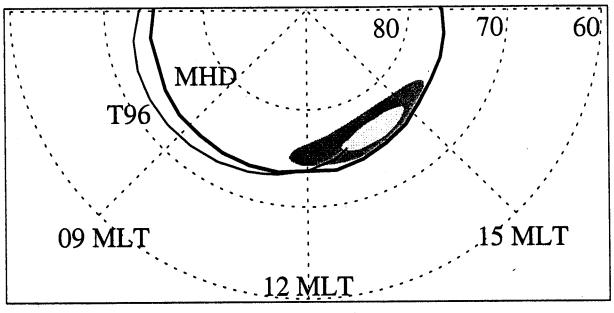

Figure 7. Magnetic local time (MLT) versus invariant latitude locations of the model dayside open-closed field line boundaries for (a) the northward IMF case, (b) the southward IMF case, and (c) the duskward IMF case. The MHD model boundaries are drawn as thick solid lines, while the T96_01 boundaries are drawn as thin solid lines. The shaded contours are the MHD 6 cm^{-3} and 10 cm^{-3} plasma density contours determined at an altitude of 6 R_E and traced down to ionospheric heights.

averaging where antiparallel field lines are forced together. In the T96_01 model the connection between solar wind and magnetospheric fields is specified by the form of the model's interconnection field. The MHD merging and strong T96_01 interconnection results in a weak or null field at the magnetopause. Note, however, that the existence of a weak or null field alone does not imply that a merging or strong interconnection region exists. Field line tracings indicating x-type neutral points or lines are also necessary to confirm the existence of MHD merging or strong T96_01 interconnection.

Figure 11 illustrates the weak magnetic field regions in the MHD model and the T96_01 model for each of the IMF directions. Each panel depicts gray scale contours of the total magnetic field magnitude within a two-dimensional slice of the magnetosphere. In the northward IMF case, Figures 11a and 11b (left), the noon-midnight plane is shown. In the southward IMF case, Figures 11a and 11b (middle), the equatorial plane is shown, and in the duskward IMF case, Figures 11a and 11b (right), the horizontal plane at a z value of 7.25 R_E and 8.25 R_E is presented for the MHD model and the T96_01 model, respectively. These planes were chosen because they contain the minimum in the total magnetic field strength. In all panels the 1 nT contour level is shaded black and represents the weakest field regions.

Numerous field line tracings (not shown) have identified that MHD merging and strong T96_01 interconnection are occurring at very localized points of null field in the northward and duskward IMF cases; see Figures 11a and 11b (left and right). However, the interconnection points in the T96_01 model are much closer to the subsolar region than are the MHD merging points, which are located tailward of the Earth near x = -4 R_E. In the MHD duskward IMF model the merging points are also well separated in the dusk-dawn direction near y = +11 R_E (y = -11 R_E) in the Northern (Southern) Hemisphere. In the southward IMF case, Figures 11a and 11b (middle), both models exhibit very weak fields all along the dayside and flank equatorial magnetopause. On the basis of field line tracings such as those depicted in Figure 9 it is found that MHD merging in the southward IMF case is occurring all along the weak field region line from dawn to dusk, while T96_01 model interconnection occurs only near the subsolar region from y = -5 R_E to y = 5 R_E. Note that the weak field regions and magnetic merging locations of the Lyon-Fedder MHD model are similar to the antiparallel magnetic field regions and magnetic merging locations identified in the MHD model of *Ogino et al.* [1986] for north, south, and y-directed IMF.

In the T96_01 model, Figure 11b, the magnetopause is identified by the transition to dark gray (or black in the southward IMF case). The field magnitudes outside the magnetopause correspond to just the interconnection field magnitudes and not true magnetosheath/solar wind magnetic field magnitudes. On the other hand, the MHD model, Figure 11a, provides a more realistic representation of the magnetic fields outside the magnetopause including a magnetosheath. For all three IMF directions the MHD bow shock is easily identified as the outer transition to darker gray. The magnetopause in the MHD model is partially identified by the narrow dark gray regions encompassing the black contours of weakest field. In the northward IMF case, Figure 11a (left), the magnetopause beyond the narrow weak field region is represented by the transition from white to gray. In the duskward IMF case, Figure 11a (right), the dark gray finger of weak field, also known as the magnetospheric sash [*White et al.*, 1998], is located only on the dusk flank of the Northern Hemisphere magnetosphere. From noon around to the dawn side the magnetopause is not discernable. Note that for the dusk IMF case the Southern Hemisphere of the magnetosphere is the mirror image of the Northern Hemisphere with the magnetospheric sash or reconnection region located only on the dawn side.

The difference in size between the two model magnetospheres is most apparent in Figure 11 with the T96_01 model magnetosphere being significantly larger. The shape and position of the T96_01 magnetopause boundary are similar to those determined from observations of

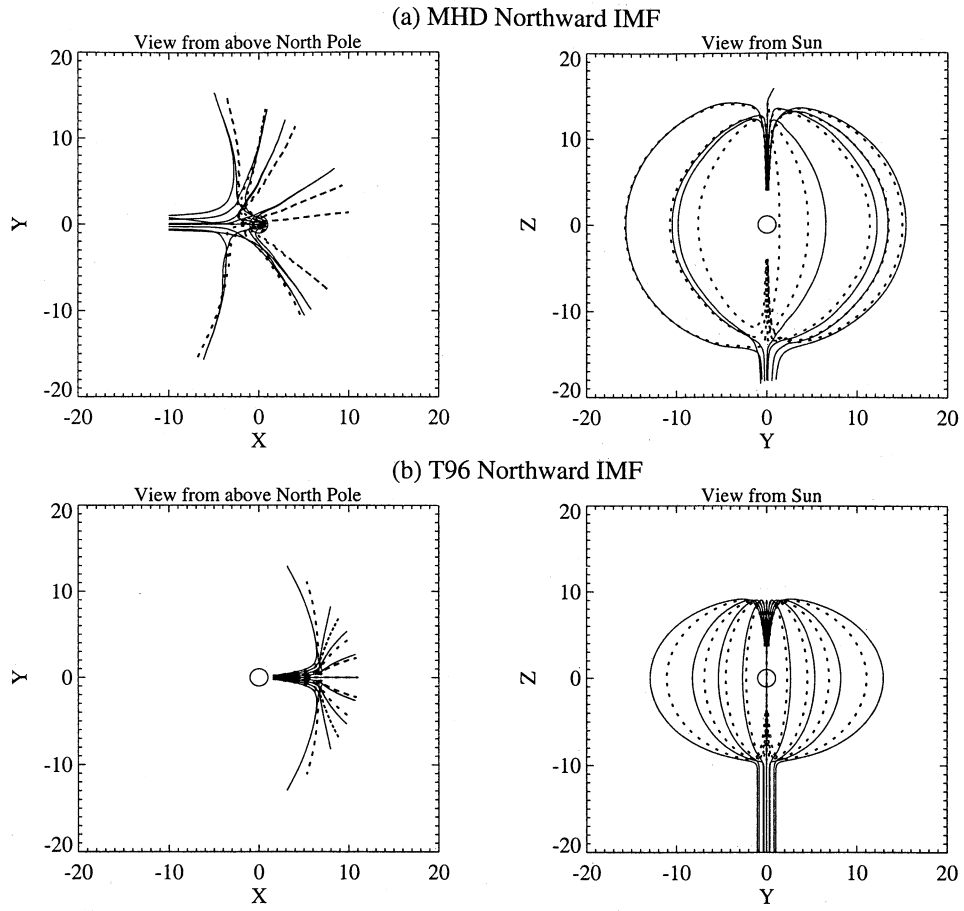

Figure 8. Northward IMF case: sample tracings of the last closed (dashed line) and first open (solid line) field lines along the Northern Hemisphere dayside open-closed field line boundary for (a) the MHD model and (b) the T96_01 model. In Figure 8a the field lines are traced in 10° increments from the noon meridian, while in Figure 8b the field lines are traced in 2° increments. Figures 8a and 8b (left) show the field lines as viewed from above the North Pole, and Figures 8a and 8b (right) show the field lines as viewed from the Sun.

magnetopause crossings by *Sibeck et al.* [1991] but do not include any variations with IMF as they are controlled only by the solar wind ram pressure. For example, the subsolar and flank locations of the T96_01 magnetopause are the same for both north and south directed IMF; see Figure 11b (left and middle). In the MHD model, Figure 11a (left and middle), the subsolar location of the magnetopause decreases from 10.5 to 9.5 R_E when going from a north directed to south directed IMF, while the flank magnetopause position does not appear to change significantly. These MHD magnetopause locations are quite consistent with the results of *Petrinec et al.* [1991] and *Sibeck et al.* [1991], except for the fact that the magnetopause flank position during southward IMF is not as large as the 20 R_E value determined by *Sibeck et al.* [1991].

4. Discussion

The results given in section 3 identify many differences between the MHD simulation model and the T96_01 empirical model, including field line configurations, cusp funnel characteristics, open-closed field line boundaries, and weak field interconnection regions. The question to be answered is which model best represents reality. A large body of observational data on the cusp region from polar orbiting satellites both at high and low altitudes is currently available for comparison with the model results. Sections 4.1 and 4.2 are a discussion of such observational results in the context of which model provides the best comparison.

4.1. Review of Case Study Comparisons

Quantitative comparisons with Polar spacecraft observations are best achieved in case studies where the time-varying solar wind conditions are input parameters to the MHD and T96_01 models. Such case studies have been completed, for example, by *Zhou et al.* [1997], *Russell et al.* [1998], and *Fedder et al.* [1997]. *Zhou et al.* [1997] studied six high-altitude passes over the North Pole comparing data from the Polar Magnetic Fields Experiment (MFE) and the T96_01 model and found that although T96_01 provided a good overall approximation to the measured fields, it was not able to predict the cusp field depressions seen in the Polar MFE measurements. This is consistent with the T96_01 model results presented here (see Figures 4, 5, and 6). Although no comparison to the MHD model was made, the range of residual magnetic field magnitude values listed in Table 1 of *Zhou et al.* [1997] encompass the MHD minimum total field residual values of approximately -40 to -50 nT seen in Figures 4c, 5c and 6c.

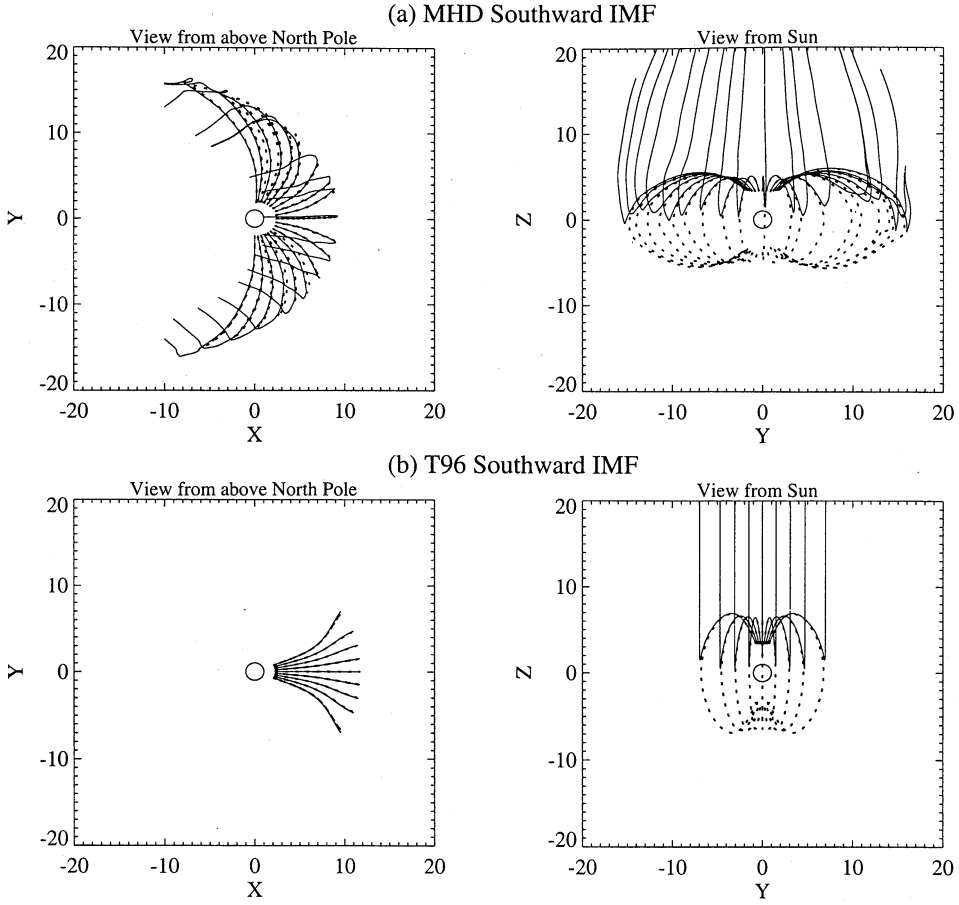

Figure 9. Southward IMF case: sample tracings of the last closed (dashed line) and first open (solid line) field lines along the Northern Hemisphere dayside open-closed field line boundary for (a) the MHD model and (b) the T96_01 model. In Figure 9a the field lines are traced in 10° increments from the noon meridian, while in figure 9b the field lines are traced in 5° increments. Figures 9a and 9b (left) show the field lines as viewed from above the North Pole, and Figures 9a and 9b (right) show the field lines as viewed from the Sun.

Russell et al. [1998] compared Polar MFE measurements to both T96_01 and the Fedder-Lyon MHD model with real solar wind inputs during a Polar cusp pass on May 29, 1996, during which the IMF was due northward. Excellent agreement was found between the Polar observations and the MHD model in terms of both magnetic field and plasma measurements. In contrast, the comparisons with the T96 model yielded significant differences primarily in the B_z and total **B** field values.

Excellent agreement between observations and the MHD model with real solar wind inputs is also shown by *Fedder et al.* [1997] during the period 1300-1700 UT, May 19, 1996. During this period the IMF rotated from dawnward to northward and then dawnward again. Throughout this event the MHD model field residuals clearly match the Polar MFE measured field residuals. In particular, the large negative B_y deflection in the cusp region is matched in magnitude. This B_y field deflection results from the passage of Polar through a field-aligned current system created by the interaction of the dawnward directed IMF with the magnetosphere and is an indication that the simulation current systems in the cusp associated with IMF B_y match those in reality. An example of such field deflections during IMF B_y can be seen in our MHD model results presented in Figures 3a (right) and 6c.

Although T96_01 has difficulty modeling the cusp region, it has been shown to do well in other locations. For example, comparisons of Polar MFE measurements with T96_01 at apogee near the terminator plane yielded very good agreement during both quiet and active periods [*Fenrich et al.*, 1998].

4.2. Comparisons With Statistical Cusp Studies

A means of testing the validity of the models is to compare the model cusp positions with positions of the cusp as determined statistically by polar-orbiting spacecraft. In a statistical study of cusp IMF dependency using low-altitude DMSP F7 satellite data, *Newell et al.* [1989] identify the cusp by high plasma number flux and low average electron and ion energies. They found that the cusp equatorward boundary lies near 78° magnetic latitude for northward IMF, B_z=+5 nT, and near 73° magnetic latitude for southward IMF, B_z=-5nT. Using Polar spacecraft measurements, *Zhou et al.* [2000] present statistical results on the solar wind control of the high-altitude cusp location. The Polar cusp crossings are identified by depressions in the magnetic field residuals and enhanced plasma densities of magnetosheath origin. *Zhou et al.* [2000] found that the equatorward boundary of the cusp lies at 78.9° invariant latitude for northward IMF, B_z=+5 nT, and lies at

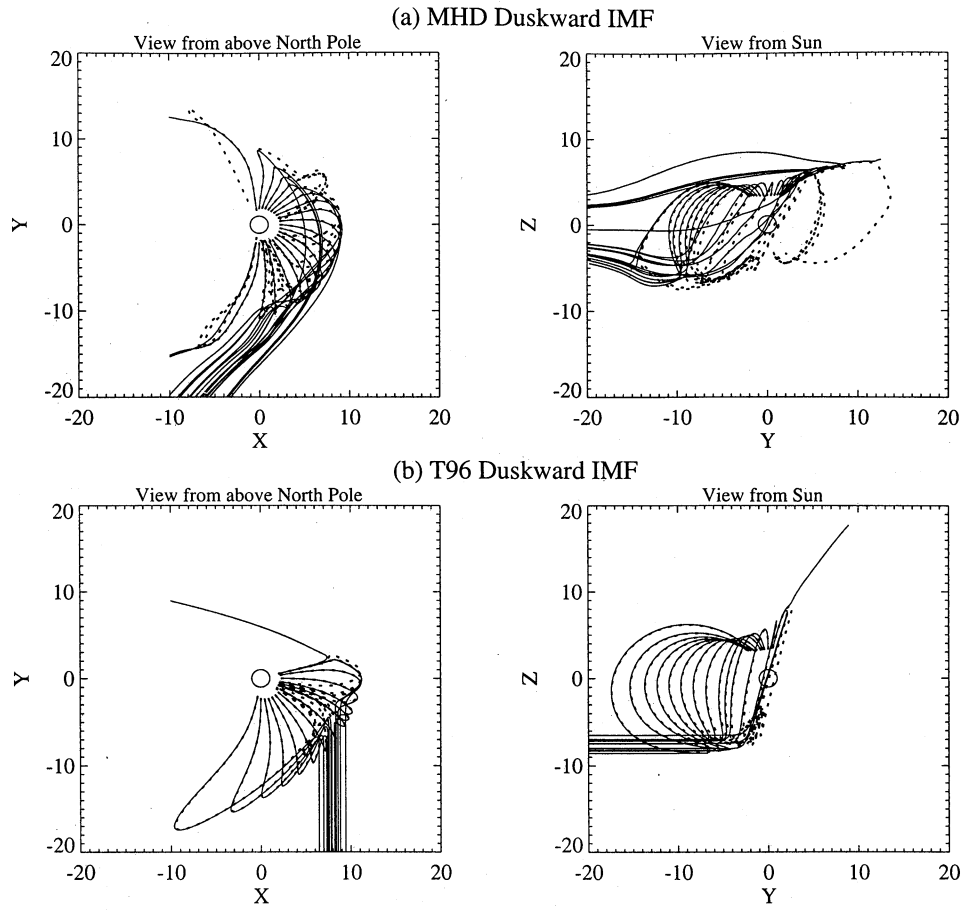

Figure 10. Duskward IMF case: sample tracings of the last closed (dashed line) and first open (solid line) field lines along the Northern Hemisphere dayside open-closed field line boundary for (a) the MHD model and (b) the T96_01 model. In Figure 10a the field lines are traced in 10° increments from the noon meridian, while in Figure 10b the field lines are traced in 10° increments reduced to 5° and 0.5° increments toward the duskward edge. Figures 10a and 10b (left) show the field lines as viewed from above the North Pole, and Figures 10a and 10b (right) show the field lines as viewed from the Sun.

75.2° for southward IMF, B_z=-5 nT. These values are ~1.5° poleward of the DMSP cusp results. Zhou et al. attribute this difference to the use of hourly average IMF in the low-altitude study in contrast to the 1-min average used in the high-altitude study. These high- and low-altitude statistics on polar cusp locations compare well with the MHD plasma cusp locations identified by the shaded regions in Figures 7a and 7b. In the case of the T96_01 model, if one assumes that the cusp plasma would accumulate in the depressed residual field regions as shown in Figures 4b and 5b, i.e., straddling the open-closed field line boundary in the north IMF case and just poleward of the open-closed boundary in the south IMF case, then the T96_01 open-closed boundary is quite consistent with the location of the statistical polar cusp for both the north and south IMF cases. If, on the other hand, the cusp plasma accumulates only on recently reconnected field lines, then in the north IMF case this would correspond to field lines equatorward of the open-closed boundary, and in this case the T96_01 model is not consistent with the statistical polar cusp for northward IMF.

In a separate study of cusp dependence on dipole tilt, *Zhou et al.* [1999] isolate the IMF B_z northward case. For dipole tilts in the range 0°-10° they show a scatterplot of cusp center positions [see *Zhou et al.* 1999, Figure 3a] which are consistent with the location of cusp field depression in the MHD model shown in Figure 4a. Of particular note is the extension of the cusp to higher altitudes in the antisunward direction for both the Polar observed cusp and the MHD cusp field depression. With respect to the T96_01 model, *Zhou et al.* [1999] found a poor fit between the Polar cusp statistics and the T96_01 model.

An IMF B_y dependence for cusp location was noted in the DMSP cusp statistics [*Newell et al.*, 1989]. In the Northern (Southern) Hemisphere the peak probability of observing the cusp shifts postnoon (prenoon) for duskward IMF. *Zhou et al.* [2000] identify a similar duskward shift of the high-altitude Northern Hemisphere cusp during periods with duskward and southward IMF components. Here again the MHD model results are consistent with the DMSP and Polar cusp statistics. As shown in Figure 7c the MHD cusp plasma shifts duskward toward later magnetic local times for dusk-directed IMF. The 1.5-2 hour shift in magnetic local time of the MHD cusp is consistent with the DMSP shift of ~1.5 hours and is slightly greater than the ~1 hour shift of the Polar cusp. The duskward shift is also consistent with antiparallel merging theories [*Crooker*, 1986, 1979; *Luhmann et al.*, 1984]. On the other

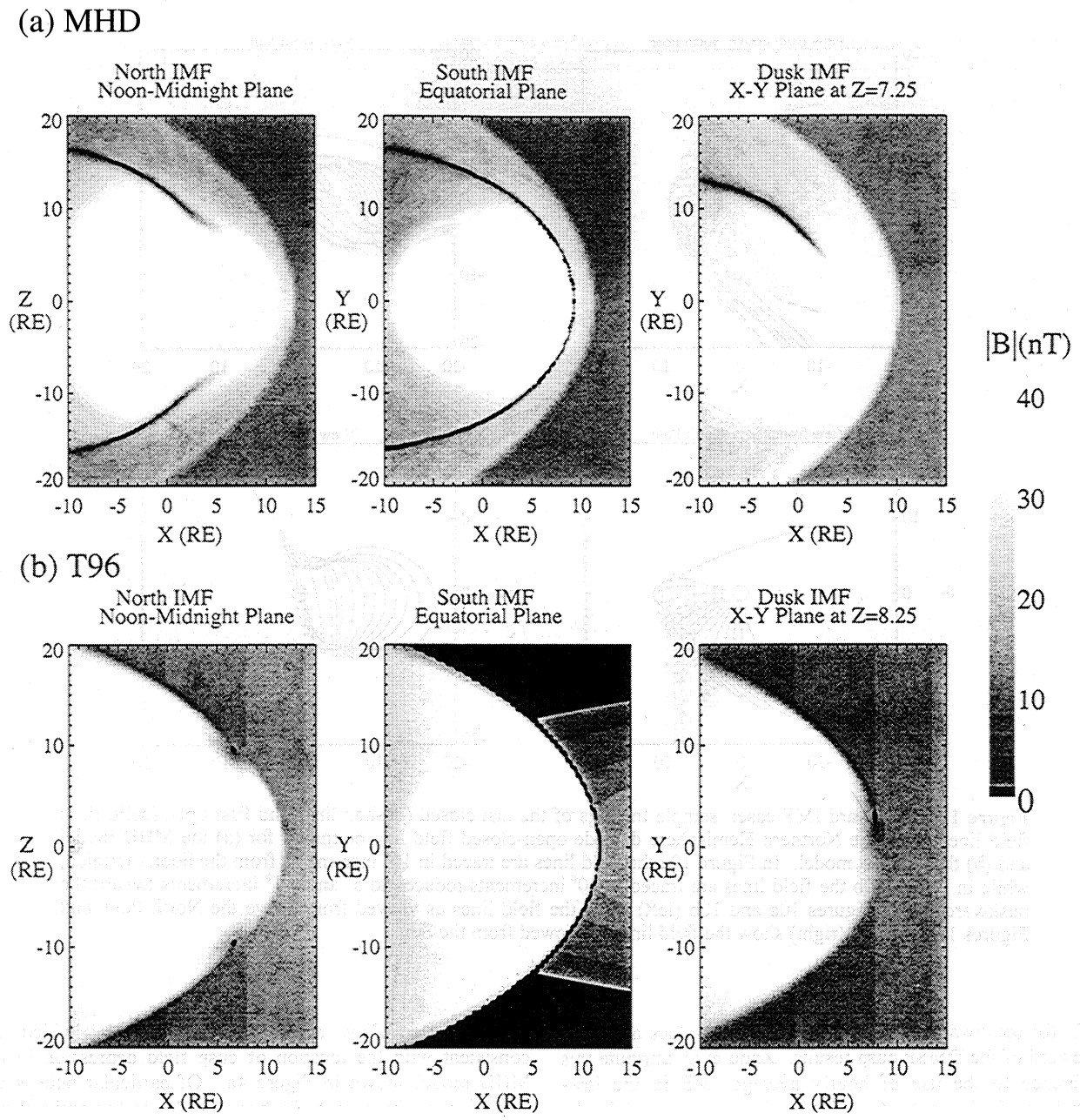

Figure 11. Shaded contour plots of the total magnetic field strength for (a) the MHD model and (b) the T96_01 model for northward (left), southward (middle), and duskward IMF (right). Figures 11a and 11b (left) show the noon-midnight plane, Figures 11a and 11b (middle) show the equatorial plane, and Figures 11a and 11b (right) show the horizontal plane at a z value of 7.25 R_E and 8.25 R_E for the MHD and T96_01 models, respectively. Note the 1 nT contour level shaded in black, which represents the weakest field region within which MHD merging and the strongest T96 interconnection occur.

hand, the T96_01 model open-closed field line boundary shifts prenoon in the Northern Hemisphere during duskward IMF (see Figure 7c), while its region of strongest interconnection at high altitude in the Northern Hemisphere shifts slightly postnoon (see Figure 11b (right)).

5. Conclusions

Dayside and flank magnetic field line configurations, cusp residual field characteristics, open-closed field line boundaries, and dayside magnetic merging and interconnection regions have been presented and compared for the Lyon-Fedder MHD simulation and the Tsyganenko 96 models for three cases of steady state solar wind conditions, i.e., for north, south, and dusk-directed IMF conditions. Many significant differences are found to exist between the two models, with both models being highly dependent upon IMF direction.

One important difference between the two models is found in the cusp residual magnetic field measurements. The MHD model exhibits strong residual total magnetic field depressions in the cusp for all IMF directions. These MHD cusp field depressions result from the diamagnetic currents of magnetosheath plasma, which has been injected into the

magnetosphere by the magnetic merging process. In the dusk-directed IMF case the MHD model also exhibits large B_y residual fields in the cusp region. Neither the large B_y residual fields during duskward IMF nor the residual total magnetic field depressions are observed in the T96_01 model. It is clear from this comparison that the cusp currents in the MHD model result are very different from those modeled in the T96_01 model.

Comparison of the two models has also identified differences between the T96_01 interconnection fields and the MHD open fields which result from MHD merging. For the northward IMF case the MHD merging of the IMF to lobe field lines near x = -4 R_E above both poles creates closed field lines of solar wind origin deep within the magnetosphere. Thus the MHD cusp plasma and diamagnetic field depression, centered near 81° invariant latitude, are well equatorward of the MHD open-closed field line boundary, which is located at 89° invariant latitude. In the T96_01 north IMF model the region of strongest interconnection is 5-6 R_E sunward of the Earth and the open-closed boundary is at 79° invariant latitude much further equatorward than that in the MHD model. In the south directed IMF case MHD merging occurs all along the equatorial dayside and flank magnetopause, but the T96_01 interconnection occurs only within ~5 R_E of the subsolar point. The southward IMF open-closed field line boundaries near noon MLT are located at 73° and 74° invariant latitude for the MHD and T96_01 models, respectively. Finally, for dusk-directed IMF, MHD merging occurs at points located ~7 R_E above (below) the equatorial plane on the dusk (dawn) flank in the Northern (Southern) Hemisphere with the open field lines in the Northern (Southern) Hemisphere threading the dawn (dusk) flank. The MHD cusp plasma and diamagnetic field depression shifts toward dusk ~1.5-2 hours in MLT in the Northern Hemisphere. For the T96_01 duskward IMF case the points of greatest interconnection are at ~8 R_E above (below) the equatorial plane and are shifted only slightly duskward (dawnward) of the noon meridian in the Northern (Southern) Hemisphere. Here, too, the open field lines in the Northern (Southern) Hemisphere connect to the dawn (dusk) side but do not extend as far back along the flanks as in the MHD model. In this case the T96_01 open-closed field line boundary spans just the dawn sector and at local noon is coincident with the MHD open-closed boundary at 74° invariant latitude.

Previous case and statistical studies of satellite observations in the cusp all provide remarkably good comparisons with the MHD cusp results while in many cases showing limited agreement with the T96_01 model. This is not surprising given the limitations of the T96_01 model as outlined in section 2. Thus, while the T96_01 model is valuable for many applications, it should be used with caution when applied to the cusp and magnetopause regions or in analyses that depend on the realism of the description of magnetic merging at the magnetopause. The MHD simulations are a more realistic description of the cusp and merging dayside magnetosphere that, at least for steady state conditions, can be made available in numerical form for general use as an alternative as was demonstrated here.

Acknowledgments. F.R. Fenrich thanks the Natural Sciences and Engineering Research Council of Canada for financial support.

Hiroshi Matsumoto thanks T. Tanaka and another referee for their assistance in evaluating this paper.

References

Crooker, N. U., Dayside merging and cusp geometry, *J. Geophys. Res., 84*, 951, 1979.

Crooker, N. U., An evolution of antiparallel merging, *Geophys. Res. Lett., 13*, 1063, 1986.

Crooker, N. U., J. G. Lyon, and J. A. Fedder, MHD model merging with IMF B_y: Lobe cells, sunward polar cap convection, and overdraped lobes, *J. Geophys. Res., 103,* 9143, 1998.

Dungey, J. W., Interplanetary field and auroral zones, *Phys. Rev. Lett., 6*, 47, 1961.

Dungey, J. W., The structure of the exosphere, or adventures in velocity space, in *Geophysics, The Earth's Environment* edited by C. DeWitt, J. Hieblot, and A. Lebeau, p. 505, Gordon and Breach, Newark, N. J., 1963.

Fedder, J. A., and J. G. Lyon, The solar wind-magnetosphere-ionosphere current-voltage relationship, *Geophys. Res. Lett., 14*, 880, 1987.

Fedder, J. A., and J. G. Lyon, The Earth's magnetosphere is 165 R_E long: Self-consistent currents, convection, magnetospheric structure, and processes for northward interplanetary magnetic field, *J. Geophys. Res., 100*, 3623, 1995.

Fedder, J. A., J. G. Lyon, C. M. Mobarry, and S. P. Slinker, Topological structure of the magnetotail as a function of interplanetary magnetic field direction, *J. Geophys. Res., 100*, 3613, 1995.

Fedder, J. A., S. P. Slinker, J. G. Lyon, C. T. Russell, F. R. Fenrich, and J. G. Luhmann, A first comparison of POLAR magnetic field measurements and magnetohydrodynamic simulation results for field-aligned currents, *Geophys. Res. Lett., 24*, 2491, 1997.

Fenrich, F. R., J. G. Luhmann, G. Le, and C. T. Russell, Polar magnetic field observations at apogee during the January 1997 magnetic cloud event, *Geophys. Res. Lett., 25*, 2541, 1998.

Gombosi, T. I., D. L. DeZeeuw, C. P. T. Groth, K. G. Powell, and P. Song, The length of the magnetotail for northward IMF: Results of a 3D MHD simulation, *Phys. Space Plasmas, 15*, 121, 1998.

Iijima, T., and T. A. Potemra, The amplitude distribution of field-aligned currents at northern high latitudes observed by Triad, *J. Geophys. Res., 81*, 2165, 1976.

Kremser, G., and R. Lundin, Average spatial distributions of energetic particles in the midaltitude cusp/cleft region observed by Viking, *J. Geophys. Res., 95*, 5753, 1990.

Luhmann, J. G., R. J. Walker, C. T. Russell, N. U. Crooker, S. R. Spreiter, and S. S. Stahara, Patterns of potential magnetic field merging sites on the dayside magnetopause, *J. Geophys. Res., 89*, 1739, 1984.

Newell, P. T., and C.-I. Meng, The cusp and cleft/boundary layer: Low-altitude identification and statistical local time variation, *J. Geophys. Res., 93*, 14,549, 1988.

Newell, P. T., C.-I. Meng, D. G. Sibeck, and R. Lepping, Some low-altitude cusp dependencies on the interplanetary magnetic field, *J. Geophys. Res., 94*, 8921, 1989.

Ogino, T., A three-dimensional MHD simulation of the interaction of the solar wind with the Earth's magnetosphere: The generation of field-aligned currents, *J. Geophys. Res., 91*, 6791, 1986.

Ogino, T., R. J. Walker, M. Ashour-Abdalla, and J. M. Dawson, An MHD simulation of the effects of the interplanetary magnetic field B_y component on the interaction of the solar wind with the Earth's magnetosphere during southward interplanetary magnetic field, *J. Geophys. Res., 91*, 10,029, 1986.

Petrinec, S. P., P. Song, and C. T. Russell, Solar cycle variations in the size and shape of the magnetopause, *J. Geophys. Res., 96*, 7893, 1991.

Raeder, J., R. J. Walker, and M. Ashour-Abdalla, The structure of the distant magnetotail during long periods of northward IMF, *Geophys. Res. Lett., 22*, 349, 1995.

Russell, C. T., J. A. Fedder, S. P. Slinker, X.-W. Zhou, G. Le, J. G. Luhmann, F. R. Fenrich, M. O. Chandler, T. E. Moore, and S. A. Fuselier, Entry of the Polar spacecraft into the polar cusp under northward IMF conditions, *Geophys. Res. Lett., 25*, 3015, 1998.

Sibeck, D. G., R. E. Lopez, and E. C. Roelof, Solar wind control of the magnetopause shape, location, and motion, *J. Geophys. Res., 96*, 5489, 1991.

Tanaka, T., Generation mechanism for magnetosphere-ionosphere current systems deduced from a three-dimensional MHD simulation of the solar wind-magnetosphere-ionosphere coupling processes, *J. Geophys. Res., 100*, 12,057, 1995.

Tanaka, T., Configuration of the magnetosphere-ionosphere convection system under northward IMF conditions with nonzero IMF B_y, *J. Geophys. Res., 104,* 14,683, 1999.

Tsyganenko, N. A., Global quantitative models of geomagnetic field in the cislunar magnetosphere for different disturbance levels, *Planet. Space Sci., 35*, 1347, 1987.

Tsyganenko, N. A., A magnetospheric magnetic field model with a warped tail current sheet, *Planet. Space Sci., 37*, 5, 1989.

Tsyganenko, N. A., Modeling the Earth's magnetospheric magnetic field confined within a realistic magnetopause, *J. Geophys. Res., 100*, 5599, 1995.

Tsyganenko, N. A., Effects of the solar wind conditions on the global magnetospheric configuration as deduced from data-based field models, in *Proceedings of the ICS-3 Conference on Substorms, Euro. Space Agency Spec. Publ., ESA-SP 389*, 181, 1996.

Tsyganenko, N. A., and D. P. Stern, Modeling the global magnetic field of the large-scale Birkeland current systems, *J. Geophys. Res., 101*, 27,187, 1996.

White, W. W., G. L. Siscoe, G. M. Erickson, Z. Kaymaz, N. C. Maynard, K. D. Siebert, B. U. O. Sonnerup, and D. R. Weimer, The magnetospheric sash and the cross-tail S, *Geophys. Res. Lett., 25*, 1605, 1998.

Zhou, X.-W., C. T. Russell, G. Le, and N. Tsyganenko, Comparison of observed and model magnetic fields at high altitudes above the polar cap: Polar initial results, *Geophys. Res. Lett., 24*, 1451, 1997.

Zhou, X.-W., C. T. Russell, G. Le, S. A. Fuselier, and J. D. Scudder, The polar cusp location and its dependence on dipole tilt, *Geophys. Res. Lett., 26*, 429, 1999.

Zhou, X.-W., C. T. Russell, G. Le, S. A. Fuselier, and J. D. Scudder, Solar wind control of the polar cusp at high altitude, *J. Geophys. Res, 105,* 245, 2000.

J. A. Fedder, Institute for Computational Sciences and Informatics, George Mason University, 4400 University Drive, Fairfax, VA 22030. (fedder@ppd.nrl.navy.mil)

F. R. Fenrich, Department of Physics, University of Alberta, 412 Avadh Bhatia Physics Laboratory, Edmonton, Alberta, Canada T6G 2J1. (frances@space.ualberta.ca)

J. G. Luhmann, Space Sciences Laboratory, University of California, Berkeley, Centennial Drive at Grizzly Peak Blvd., Berkeley, CA 94720-7450. (jgluhman@ssl.berkeley.edu)

C. T. Russell, Institute of Geophysics and Planetary Physics, University of California, 3845 Slichter Hall, 405 Hilgard Avenue, Los Angeles, CA 90095-1567. (ctrussel@igpp.ucla.edu)

S. P. Slinker, Plasma Physics Division, Naval Research Laboratory, Code 6794, Washington, D. C. 20375-5320. (slinker@ppdu.nrl.navy.mil)

(Received March 7, 2000; revised March 22, 2001;
accepted March 22, 2001.)